MNRAS 000, 1–8 (2017) Preprint 27 August 2018 Compiled using MNRAS LATEX style file v3.0

Deep-Down Ionization of Protoplanetary Disks

A. E. Glassgold[1⋆], S. Lizano[2], D. Galli[3]
[1]*Astronomy Department, University of California, Berkeley, CA 94720, USA*
[2]*Instituto de Radioastronomía y Astrofísica, UNAM, Apartado Postal 3-72, 58089 Morelia, Michoacán, México*
[3]*INAF-Osservatorio Astrofisico di Arcetri, Largo E. Fermi 5, 50125 Firenze, Italy*

Accepted 2017 August 15. Received 2017 August 15; in original form 2017 June 29

ABSTRACT

The possible occurrence of dead zones in protoplanetary disks subject to the magneto-rotational instability highlights the importance of disk ionization. We present a closed-form theory for the deep-down ionization by X-rays at depths below the disk surface dominated by far-ultraviolet radiation. Simple analytic solutions are given for the major ion classes, electrons, atomic ions, molecular ions and negatively charged grains. In addition to the formation of molecular ions by X-ray ionization of H_2 and their destruction by dissociative recombination, several key processes that operate in this region are included, e.g., charge exchange of molecular ions and neutral atoms and destruction of ions by grains. Over much of the inner disk, the vertical decrease in ionization with depth into the disk is described by simple power laws, which can easily be included in more detailed modeling of magnetized disks. The new ionization theory is used to illustrate the non-ideal MHD effects of Ohmic, Hall and Ambipolar diffusion for a magnetic model of a T Tauri star disk using the appropriate Elsasser numbers.

Key words: ISM: abundances – protoplanetary disks – magnetohydrodynamics

1 INTRODUCTION

Twenty-five years ago Balbus & Hawley (1991) proposed a little known instability in rotating magnetized disks, the magnetorotational instability (MRI), that might explain how accretion and turbulence occur in protoplanetary disks (PPDs). Gammie (1996) stressed how important the level of ionization is for the operation of the MRI. Assuming that PPDs are permeated by interstellar cosmic rays, he showed how too little ionization can lead to so-called dead zones where the MRI does not occur, usually close to the mid-plane. It was then argued that the cosmic rays could easily be blocked by the strong winds of young stellar objects, and that X-rays could ionize PPDs (Glassgold, Najita & Igea 1997).

Our understanding of disk ionization is still incomplete for a variety of technical and physical reasons. Although considerable progress has been made in both theoretical and observational studies of the warm surface layers of PPDs irradiated by stellar far-ultraviolet (FUV) radiation (reviewed by Najita & Ádámkovics 2017), little is known about regions closer to the mid-plane where no clear diagnostics have been identified so far. The underlying physics of both X-ray and cosmic-ray ionization of the inner disk is also incomplete. The Monte-Carlo calculations of X-ray absorption and scattering (e.g., Igea & Glassgold 1999; Ercolano & Glassgold 2013) become inaccurate beyond a certain depth into the disk, e.g., for vertical column densities $N_{\rm H}$ with $\log N_{\rm H} > 25.25$. In addition, there is the issue of the blocking of the cosmic rays by a strong, asymmetric stellar wind. Cleeves et al. (2013) first approached this problem and obtained CR ionization rates 1000 smaller than the interstellar value due to the modulation of the cosmic rays by the T Tauri star wind.

Thermal-chemical models of the disks surface often involve hundreds of species and thousands of reactions, and as such are unsuitable for inclusion with 2-d and 3-d solutions of the non-ideal MHD equations. This difficulty can be overcome by resorting to the simplified treatment used by Oppenheimer & Dalgarno (1974) for ionization in dark clouds, and applied to PPDs by Ilgner & Nelson (2006a,b) and Bai & Goodman (2009). In this approach, the ionization theory treats only a small set of generic species, e.g., molecular ions like HCO^+ and H_3O^+ (represented by m^+), heavy atomic ions like Na^+ and Mg^+ (represented by M^+), and charged grains (g^-). This formulation still allows for the proper treatment of the destruction of molecular ions by including charge-transfer to heavy atoms as well as dissociative recombination with electrons, with the subsequent destruction of the heavy atomic ions by recombination on charged grains. We adopt this perspective, following Ilgner & Nelson and Bai & Goodman.

⋆ aglassgold@berkeley.edu

We focus on the ionization of the inner part of a PPD below the surface layer dominated by FUV ionization, and assume that the disk has experienced significant grain growth. The goal is to track the ionization down to the mid-plane, which we refer to as "deep-down" ionization. An important element of the theory is the approximate power-law dependence of the X-ray ionization parameter, $\tilde{\zeta} \equiv \zeta_X/n_{\rm H}$ on vertical column density $N_{\rm H}$, where ζ_X is the ionization rate and $n_{\rm H}$ is the number density of hydrogen nuclei. This leads to simple power laws for the ion abundances, relations that can be easily accommodated in MHD calculations of disks. We illustrate these results by considering all three non-ideal MHD effects (Ohmic, Hall and Ambipolar) for a weakly-magnetized disk model of Lizano et al. (2016) for the T Tauri star disk.

Although the theory presented in this paper provides a significant simplification of PPD ionization, many unknowns remain. The exact level of both X-ray and cosmic-ray ionization approaching close to the mid-plane are uncertain, and the role of mixing needs to be considered. In addition, the choice of important physical parameters like the X-ray luminosity, the grain surface area, and the gaseous heavy-element abundance can affect the character of the ionization. The importance of disk ionization goes beyond considerations of the MRI because in general it determines the coupling of the field to the disk ions and the coupling of the ions to the neutral species, essential issues for any theory of magnetized disks.

2 PHYSICAL PROCESSES AND SOLUTION

We apply the Oppenheimer & Dalgarno (1974) method to PPDs by first writing balance equations for the number density of molecular and atomic ions, $n(m^+)$ and $n(M^+)$,

$$\zeta_X n_{\rm H} = (k n_M + \beta n_e + k_d n_d)\, n(m^+), \tag{1}$$

$$k_{\rm ce} n_M n(m^+) = (\alpha n_e + k_d n_d)\, n(M^+). \tag{2}$$

Eq. (1) expresses the idea that the ionization is due to X-ray ionization of H_2 and that the proton in H_2^+ is rapidly transferred to high-abundance molecules that better bind the proton, especially CO and H_2O. The right side of the equation states that the molecular ions can be lost by charge exchange with neutral atoms, dissociative recombination with electrons, and recombination with grains. In this equation, the rate coefficient, $k = k_{\rm ce} + k_{\rm pt}$, is the sum of charge-exchange and proton-transfer rate coefficients for atomic ions reacting with molecular hydrogen; n_M, n_e and n_d are the number density of neutral atoms, electrons, and dust, respectively. Eq. (2) describes how atomic ions are produced by charge exchange of molecular ions with neutral atoms and how they can be destroyed by either recombination with grains or electrons. The rate coefficients α and β have their usual values (Spitzer 1978, Anicich 1993),

$$\alpha = 2\times10^{-10}\, T^{-2/3}\,{\rm cm^3\,s^{-1}},\ \beta = 1.2\times10^{-7}\, T^{-3/4}\,{\rm cm^3\,s^{-1}}. \tag{3}$$

The information available on the reaction of molecular ions with atoms is limited, and we estimate that the rate coefficient for charge exchange and proton transfer are about the same and equal to,

$$k_{\rm ce} = k_{\rm pt} = 5\times10^{-10}\,{\rm cm^3\,s^{-1}}. \tag{4}$$

The grains are treated according to the collisional-charging theory of Draine & Sutin (1987, hereafter DS87). For a typical grain size a (e.g., the geometric mean of the minimum and maximum sizes in the Mathis et al. 1977 $a^{-3.5}$ power law distribution[1]), DS87 introduce an "effective temperature"

$$\tau = \frac{a k_{\rm B} T}{e^2} = 59.9 \left(\frac{a}{10\ \mu{\rm m}}\right)\left(\frac{T}{100\ {\rm K}}\right), \tag{5}$$

and an "effective atomic weight" of the ions μ_i defined by their Eq. (4.8b). Assuming an "electron sticking coefficient" $s_e = 1$, μ_i is given by

$$\mu_i \equiv \left(\frac{n_e}{n_i}\right)^2 \left(\frac{m_i}{m_{\rm H}}\right), \tag{6}$$

where the total ion density is

$$n_i = n(M^+) + n(m^+), \tag{7}$$

and the average ion mass m_i is given by

$$\frac{n_i}{m_i^{1/2}} = \frac{n(M^+)}{m_M^{1/2}} + \frac{n(m^+)}{m_m^{1/2}}. \tag{8}$$

Assuming an ion mass, $m_k = A_k m_{\rm H}$, with $k = M, m$, the effective atomic weight can be written as

$$\mu_i = {n_e}^2 \left[\frac{n(M^+)}{A_M^{1/2}} + \frac{n(m^+)}{A_m^{1/2}}\right]^{-2} \tag{9}$$

The grain charge depends only on τ and μ_i. While τ depends on grain size and temperature, μ_i is bound by two limiting values: if dust plays no role in the charge balance, $n_i \approx n_e$ and $\mu_i \approx \langle A_i\rangle$, where $\langle A_i\rangle \approx 25$. Instead, if the grains carry free charge, as a consequence of balance between negatively and positively charged grains, $n_i/n_e \approx (\langle A_i\rangle m_{\rm H}/m_e)^{1/2}$ and $\mu_i \approx m_e/m_{\rm H}$ (see, e.g., Eq. 28 of Nakano et al. 2002). In the limit of the big grains/high temperatures of interest here ($\tau \gg 1$) the grain charge is given by

$$\langle Z_d\rangle \approx -\tau\psi, \tag{10}$$

where ψ is the solution of the charge equation (Spitzer 1941)

$$(1+\psi)e^{\psi} = \sqrt{\frac{\mu_i m_{\rm H}}{m_e}}, \tag{11}$$

and m_e is the mass of the electron. For electron and heavy atoms with $m_M = 25 m_{\rm H}$, $\psi = 3.8$, but if grains dominate the negative charge, ψ will be much smaller. In the example treated below, $\psi < 1$ near the mid-plane. In applying the DS87 theory to the present problem, we assume that the grains and the temperature are large enough for the effective temperature in Eq. (5) to satisfy $\tau \gg 1$.

The contribution of the grains to the total charge fraction (g^-) is then,

$$\begin{aligned} x(g^-) = &\quad -x_d\langle Z_d\rangle \\ = &\quad 1.12\times10^{-16}\left(\tfrac{\rho_g/\rho_d}{0.01}\right)\left(\tfrac{10\mu{\rm m}}{a}\right)^2\left(\tfrac{T}{100{\rm K}}\right)\psi, \end{aligned} \tag{12}$$

[1] We adopt $10\,\mu$m as representative grain size, but the formulae allow for consideration of other sizes.

where the dust abundance relative to the density of H nuclei is,

$$x_d = \frac{n_d}{n_{\rm H}} = 1.863\times10^{-18}\left(\frac{\rho_g/\rho_d}{0.01}\right)\left(\frac{a}{10\,\mu{\rm m}}\right)^{-3}. \quad (13)$$

DS87 also give approximate expressions for the recombination rate coefficient k_d for the reaction of heavy ions, both atomic and molecular, with grains,

$$k_d \approx \pi a^2 \langle v_i\rangle\,(1+\psi)\,, \quad (14)$$

where the mean thermal ion speed is $\langle v_i\rangle = \sqrt{8k_{\rm B}T/\pi\langle A_i\rangle m_{\rm H}}$. This rate can be written as

$$k_d = 9.11\times10^{-2}\left(\frac{a}{10\,\mu{\rm m}}\right)^2\left(\frac{T}{100\,{\rm K}}\right)^{1/2}(1+\psi)\ {\rm cm^3\,s^{-1}}. \quad (15)$$

The grain destruction term in eqs. (1) and (2) is then,

$$k_d\,x_d = 1.70\times10^{-19} D\ {\rm cm^3\,s^{-1}}, \quad (16)$$

with

$$D = \left(\frac{\rho_g/\rho_d}{0.01}\right)\left(\frac{10\,\mu{\rm m}}{a}\right)\left(\frac{T}{100\,{\rm K}}\right)^{1/2}. \quad (17)$$

The basics of the ionization theory can now be completed with the equation for charge conservation,

$$n(m^+) + n(M^+) = n_e + n(g^-). \quad (18)$$

It is then straightforward to obtain formulae for abundances of m^+ and M^+,

$$x(M^+) = \frac{k_{\rm ce}\,x_M[x_e + x(g^-)]}{k_{\rm ce}\,x_M + k_d\,x_d + \alpha\,x_e}, \quad (19)$$

$$x(m^+) = \frac{(k_d\,x_d + \alpha x_e)[x_e + x(g^-)]}{k_{\rm ce}\,x_M + k_d\,x_d + \alpha x_e}, \quad (20)$$

and then obtain a cubic equation for the electron fraction,

$$\begin{aligned}&\alpha\beta x_e^3 + [\alpha(k\,x_M + k_d\,x_d) + \beta x_d(k_d - \alpha\langle Z_d\rangle)]x_e^2\\ &\quad -\{\tilde\zeta\,\alpha - k\,x_M\,x_d(k_d - \alpha\langle Z_d\rangle) + x_d^2\,[(\alpha+\beta)\,\langle Z_d\rangle - k_d^2\,]\}x_e\\ &\quad -[\tilde\zeta\,(k_{\rm ce}\,x_M + k_d\,x_d) + k_d\,x_d^2\,k\,x_M\,\langle Z_d\rangle + k_d^2\,x_d^3\,\langle Z_d\rangle] = 0. \quad (21)\end{aligned}$$

In principle, Eq. (21) can be adapted to treat high as well as low ionization regions of PPDs. The ionization rate ζ_X would then have to include a broader range of external radiation than just the energetic X-rays considered here. In particular, the surface layers are strongly affected by FUV radiation, including Lyman-α. As shown in recent models of the inner surface layers, e.g., Ádámkovics et al. (2014, 2016), shielding by dust and molecules play an essential role in determining the effects of FUV irradiation. In this report, we focus on that part of the PPD that lies below the FUV layer where the ionization is many orders of magnitude less than near the surface. In this deep-down region of a PPD, the X-ray ionization rate plays a key role in determining the ionization. It enters the cubic equation Eq. (21) through the ionization parameter, $\tilde\zeta$. As discussed in earlier work (Igea & Glassgold 1999; Ercolano & Glassgold 2013), the penetration of the X-rays to large depths depends on their scattering by electrons, both free and weakly bound. These studies show that the X-ray ionization parameter in the inner PPD (out to $R \approx$ 15-20 AU) decreases rapidly with height and relatively slowly with radius. For the MMSN, the decrease follows the $-8/3$ power of the vertical column density $N_{\rm H}$ (measured from the top),

$$\tilde\zeta = \zeta_X/n_{\rm H} = 10^{-33}\,(N_{\rm H}/10^{26}\,{\rm cm^{-2}})^{-8/3}\,{\rm cm^3\,s^{-1}}. \quad (22)$$

This behavior is also expected to apply to other density distributions[2]. However, our understanding of X-ray ionization is incomplete at the largest depths in PPDs (approaching the mid-plane) because of the limitations in the Monte Carlo scattering calculations. In practice this means that the X-ray ionization rates are uncertain for vertical columns greater than $\log N_{\rm H} = 25.25$.

The ionization level in the regions of interest for this work are small, $< 10^{-9}$, and even smaller approaching the mid-plane. Under these conditions, the quadratic and cubic terms in Eq. (21) can be ignored, as can the quadratic and cubic terms in x_d in the last two terms of the equation. In addition, the terms involving the radiative recombination coefficient α can be dropped, leading to a simple expression for the electron fraction deep down in the inner part of a PPD,

$$x_e \approx \tilde\zeta\,\frac{k_{\rm ce}\,x_M + k_d\,x_d}{k\,x_M\,k_d\,x_d}. \quad (23)$$

The relative size of the two terms in the numerator depend on the abundance of heavy atoms in the gas phase ($k_{\rm ce}\,x_M$) and on the abundance and size of the grains ($x_d\,k_d$ from Eq. 16). To estimate the order of magnitude of these terms, Eq. (23) can be rewritten using Eq. (16) with $T = 100$ K and $\rho_g/\rho_d = 0.01$, as

$$\frac{k_{\rm ce}\,x_M + k_d\,x_d}{k\,x_M\,k_d\,x_d} \approx \left[\frac{2.9\times10^{18}}{1+\psi}\left(\frac{a}{10\,\mu{\rm m}}\right) + \frac{10^9}{x_M}\right]{\rm cm^{-3}\,s}. \quad (24)$$

The abundance of heavy atoms x_M determines the size of the second term of this equation. Other than several well studied lines of sight for diffuse clouds (e.g. Savage & Sembach 1996), little is known about the abundance of gas phase heavy atoms in thicker clouds and protoplanetary disks. In diffuse clouds, the volatile atoms Na and K are depleted by about 1 dex, Mg and Si by 1.5 dex, the more refractory Fe by ~ 230, and essentially no depletion for S. A study of abundances for five thicker clouds by Joseph et al. (1986) yielded a larger depletion for Si and a 1 dex depletion for S. More recently, Anderson et al. (2013) measured the 25 μm S I fine-structure emission from three Class 0 sources with outflows and shocks. They obtain lower and upper limits for the depletion of atomic S, which they interpreted as produced by shock-induced vaporization of sulfur-rich grain mantles. There is no new information on the abundance of Na and K. We adopt a conservative approach to this fragmentary observational situation by adopting the largest depletion factors suggested for Na (10), Mg (40), Si (75), S (100), K (12) and Fe (180). The average abundance of these heavy atoms is then $x_M = 1.8\times10^{-6}$, close to the undepleted, solar Na abundance. This number might well be smaller because it relies heavily on the uncertain depletions of Mg and Si. Our

[2] The slow decrease of $\tilde\zeta$ with R may be understood from the fact that both ζ_X and $n_{\rm H}$ decrease as the inverse square of the radius. The deep-down variation of $\tilde\zeta$ with column density in Eq. (22) stems from the fact that ζ_X varies with $N_{\rm H}$ slightly less strongly than R^{-2} and $n_{\rm H}$ varies with $N_{\rm H}$ slightly less strongly than R^{-1}.

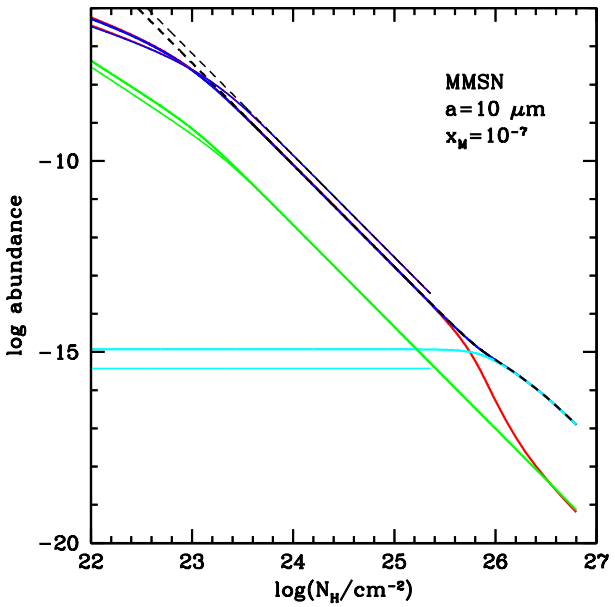

Figure 1. Abundances as function of vertical column density for a MMSN disk at $R = 1$ AU and 10 AU, for grains with size $a = 10\,\mu$m, and heavy atom abundance $x_M = 10^{-7}$. The curves are for x_e (*red*), $x(M^+)$ (*blue*), $x(m^+)$ (*green*), and $x(g^-)$ (*cyan*). The *dashed black curves* correspond to the simple analytic solution, Eq. (25). The thicker lines correspond to $R = 1$ AU; these lines reach the highest column density ($N_H = 7.2 \times 10^{26}\,\mathrm{cm}^{-2}$). The curves shift slightly with R in accord with the decline in the temperature of the isothermal atmosphere of the MMSN.

best conservative guess is $x_M = 10^{-7}$, or 0.1% of the solar abundance. If we use this value in Eq. (24), we find that the second term is between 1 and 2 dex smaller that the first, unless the effective grain size (surface area) is very small, i.e, less than 0.1μm. Where the second term can be ignored, Eq. (23) becomes,

$$x_e \approx \tilde{\zeta}\,\frac{k_{\rm ce}/k}{k_d\,x_d} = 0.5\frac{\tilde{\zeta}}{k_d\,x_d}, \tag{25}$$

directly expressing how the electron fraction is determined by the ion production by X-rays and destruction by grains (see also Eq. (58) of Okuzumi & Inutsuka 2015). This equation should suffice for a preliminary discussion of deep-down ionization.

3 RESULTS FOR ION ABUNDANCES

We illustrate the theory presented in the previous section by applying it to the Minimum Mass Solar Nebula (MMSN, Hayashi 1981)[3]. The reference case is defined by a grain size of $a = 10\,\mu$m and a heavy atom abundance $x_M = 10^{-7}$. Figure 1 shows the solution of the cubic equation Eq. (21) for a disk radius $R = 1$ AU with abundances plotted against vertical column density in the range $\log N_{\rm H} = 22$–26. The main ions, e, M^+, m^+ and g^-, all follow power laws to a good approximation. The ionization is largely dominated by the relation $x_e = x(M^+)$. The molecular ions follow a parallel line but down by 1.5 dex. The negative grain abundance in this case is approximately constant at $x(g^-) \approx 10^{-15}$. It plays no role until close to the mid-plane of the disk where it becomes more abundant than electrons. The simple analytic abundance formula, Eq. (25), is represented by a dashed line. It agrees closely with the solution to the cubic except at small columns where the straight line fit begins to fail, and also at the largest columns where negatively-charges grains replace electrons as the major carrier of negative charge. The relatively high electron abundance at small columns is due to X-ray ionization producing high abundances of heavy atomic ions, the basis for the present theory of ionization deep down. In a more complete theory of disk ionization, x_e will be even larger at small columns due to FUV ionization. The electron fraction generally follows the $-8/3$ power dependence of the ionization parameter $\tilde{\zeta}$ in Eq. (22). Figure 1 also shows the ion abundances for the disk radius $R = 10$ AU. There is a small decrease in ionization with increasing radius. This is due to the decline with radius of the temperature of the isothermal atmospheres in the MMSN. The numerator in the second factor of Eq. (25) is assumed to be fixed at 0.5, and the denominator $k_d\,x_d$ does not change with grain size because grain size has been fixed in this figure. The term $k_d\,x_d$ does produce the small variation with radius via its temperature dependence, according to Eq. (16). The grain charge also decreases with decreasing temperature, according to Eq. (12).

The behavior of the ions can be understood by examining Eq. (19) and Eq. (20) for M^+ and m^+. The denominators of both equations are dominated by the first term, $k_{\rm ce}\,x_M$. Applying $x(g^-) \ll x_e$ in the numerator of Eq. (19), then leads to $x(M^+) = x_e$, in agreement with the figure. Ignoring small terms in the numerator of Eq. (20) then leads to,

$$x(m^+) = \frac{k_d\,x_d}{k_{\rm ce}\,x_M}\,x_e, \tag{26}$$

so that $x(m^+)$ is both proportional to but much smaller than x_e, as shown in the figure.

Figure 2 displays the dependence on grain size and heavy atom abundance obtained with the cubic Eq. (21) at 1 AU. The general increase of $x_e = x(M^+)$ in Figure 2 is in accord with the simple ionization theory of the previous section, where $x_e \propto a$, using Eqs. (25) and (16). Likewise, $x(g^-)$ decreases because, referring to Eq. (12), it is inversely proportional to a^2. By contrast, $x(m^+)$ is independent of grain size because according to Eq. (20), the dependence on grain size of the two factors, $k_d\,x_d$ and x_e, cancel. However, among all of the species under discussion, m^+ is the only one sensitive to the heavy element abundance, as shown in Figure 2 and predicted by Eq. (20).

4 APPLICATION TO MAGNETIC DISKS

We calculate the non-ideal MHD diffusivities in the low-ionization limit given in Appendix B of Pinto, Galli &

[3] The MMSN parameters at 1 AU are: temperature, 280 K; scale height, 5×10^{11} cm; and mid-plane density, $1.15 \times 10^{15}\,\mathrm{cm}^{-3}$; the mass column of H nuclei is then $1700\,\mathrm{g\,cm}^{-2}$; the mid-plane temperature and density vary with radius as the -0.5 and -2.75 powers, respectively.

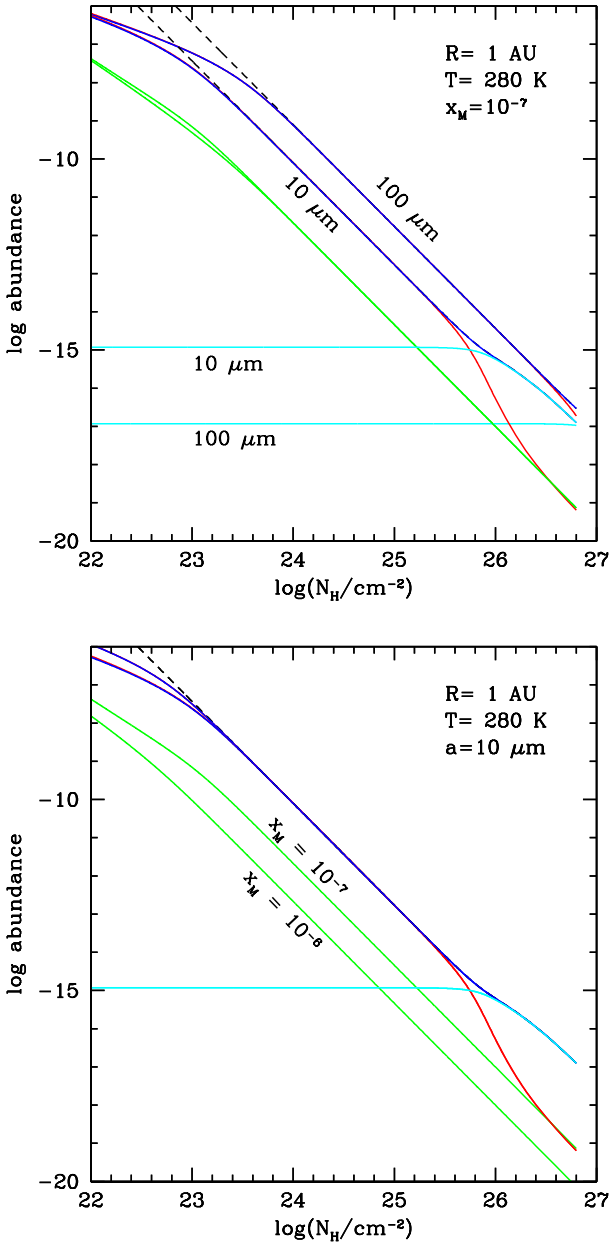

Figure 2. *Top panel:* Variation with grain size, $a = 10, 100\,\mu$m. *Bottom panel:* Variation with heavy atom abundances, $x_M = 10^{-6}, 10^{-7}$. The curves have the same meaning as in Figure 1.

Bacciotti (2008), using the rate coefficients in Pinto & Galli (2008a,b). The last equations of this appendix for the case where the charged particles are electrons and heavy ions lead to these familiar forms for the Ohmic (O), Hall (H) and Ambipolar Diffusion (AD) diffusivities,

$$\eta_{\rm O} = \frac{1}{4\pi r_e}\,\frac{\langle\sigma v\rangle_{e,n}}{x_e} \tag{27}$$

$$\eta_{\rm H} = \frac{cB}{4\pi e n_e} \tag{28}$$

$$\eta_{\rm AD} = \frac{B^2}{4\pi\gamma_{i,n}\,\rho_i\,\rho_n} \approx \frac{v_{\rm A}^2}{n_{\rm H}\langle\sigma v\rangle_{i,n}\,x_i} \tag{29}$$

where $r_e = 2.818\times10^{-13}$ cm is the classical electron radius, $\langle\sigma v\rangle_{e,n}$ and $\langle\sigma v\rangle_{i,n}$ are average rate coefficients for electron- and ion-neutral momentum transfer, c is the speed of light, $\rho_n = n_{\rm H}\,m_{\rm H}$, $\gamma_{i,n}\rho_i \approx n_{\rm H}\,x_i\,\langle\sigma v\rangle_{e,n}$, and $v_{\rm A}$ is the Alfvén velocity,

$$v_{\rm A} = \frac{B}{\sqrt{4\pi\rho}} = 1.84\times10^{11}\left(\frac{B}{G}\right)\left(\frac{n_{\rm H}}{\rm cm^{-3}}\right)^{-1/2}\,{\rm cm\,s^{-1}}. \tag{30}$$

The temperature dependence of $\langle\sigma v\rangle_{e,{\rm H}_2}$ is obtained from Table 1 of Pinto & Galli (2008b); typical values for this rate coefficient are $\sim 10^{-8}\,{\rm cm^3\,s^{-1}}$. Now using Eq. (A.5) of Pinto & Galli (2008b), $\langle\sigma\,v\rangle_{M^+,{\rm H}_2} = 1.85\times10^{-9}\,{\rm cm^3\,s^{-1}}$, independent of temperature, taking the heavy atom mass to be $25\,m_{\rm H}$.

We evaluate the diffusivities and related quantities for the vertical structure of a weakly-magnetized disk model around a T Tauri star (Lizano et al. 2016). The disk is threaded by a poloidal magnetic field dragged in from the parent core during the phase of gravitational collapse (Shu et al. 2007). This model has a a viscosity coefficient $D = 10^{-2.5}$ and a dimensionless mass-to-flux ratio $\lambda = 2\pi G^{1/2}(M_* + M_d)/\Phi = 12$, where the stellar mass is $M_* = 0.5\ M_\odot$ and the disk mass is $M_d = 0.03\ M_\odot$. The disk radius is $R_d = 39.3$ AU and the mass accretion rate is $\dot{M} = 10^{-8}\ M_\odot\ {\rm yr^{-1}}$. The radial surface density distribution is $\Sigma_R = 540.3\,(R/{\rm AU})^{-3/4}$ g cm^{-2} (half above and half below the mid-plane). The aspect ratio is $A = 0.033\,(R/{\rm AU})^{1/4}$. The vertical magnetic field component is $B_z = 6.1\,(R/{\rm AU})^{-11/8}$ G, and the radial component is $B_R = 2B_R^+\,(\Sigma/\Sigma_R)$ where $B_R^+ = 1.742\,B_z$ is the radial field at the disk surface. The disk is internally heated by viscous and resistive dissipation and its surface is irradiated by the central star.

The focus is on intermediate altitudes below the FUV zone and extending down close to the mid-plane. Here the dominant neutral is molecular hydrogen, and the ionization parameter $\tilde{\zeta}$ varies approximately as $N_{\rm H}^{-8/3}$. The dependence of the ionization fractions on column density is obtained with the theory described in Sec. 2. In order to better understand the numerical values of the diffusivities, we also calculate the corresponding Elsasser numbers using the Keplerian rotation frequency, $\Omega(R) = 1.4\times10^{-7}\,(M_*/0.5M_\odot)^{1/2}\,(R/{\rm AU})^{-3/2}$ s^{-1},

$${\rm Am_O} = \frac{c_s^2}{\Omega\,\eta_{\rm O}} \qquad {\rm Am_H} = \frac{v_{\rm A}^2}{\Omega\,\eta_{\rm H}} \qquad {\rm Am_{AD}} = \frac{v_{\rm A}^2}{\Omega\,\eta_{\rm AD}}, \tag{31}$$

where c_s is the isothermal sound speed for a molecular-hydrogen plus helium mixture, $c_s = 6.00\times10^4\,(T/100{\rm K})^{1/2}$ cm s^{-1} and the Alfvén velocity $v_{\rm A}$ is given above in Eq. (30). For the Hall term, we can also use a spatial scale closely related to the Elsasser number, i.e., the so-called Hall length (e.g., Lesur et al. 2014),

$$L_{\rm H} = \frac{\eta_{\rm H}}{v_{\rm A}} = \frac{v_{\rm A}}{\Omega}\,\frac{1}{{\rm Am_H}}. \tag{32}$$

Lesur et al. (2014) interpret $L_{\rm H}$ as a measure of the spatial range of the Hall effect. The unique characterizations of the non-ideal MHD terms in Eqs. (31) and (32) arise from the different dependences of the original diffusivities, Eqs. (27), (28) and (29), on ionization fraction and magnetic field.

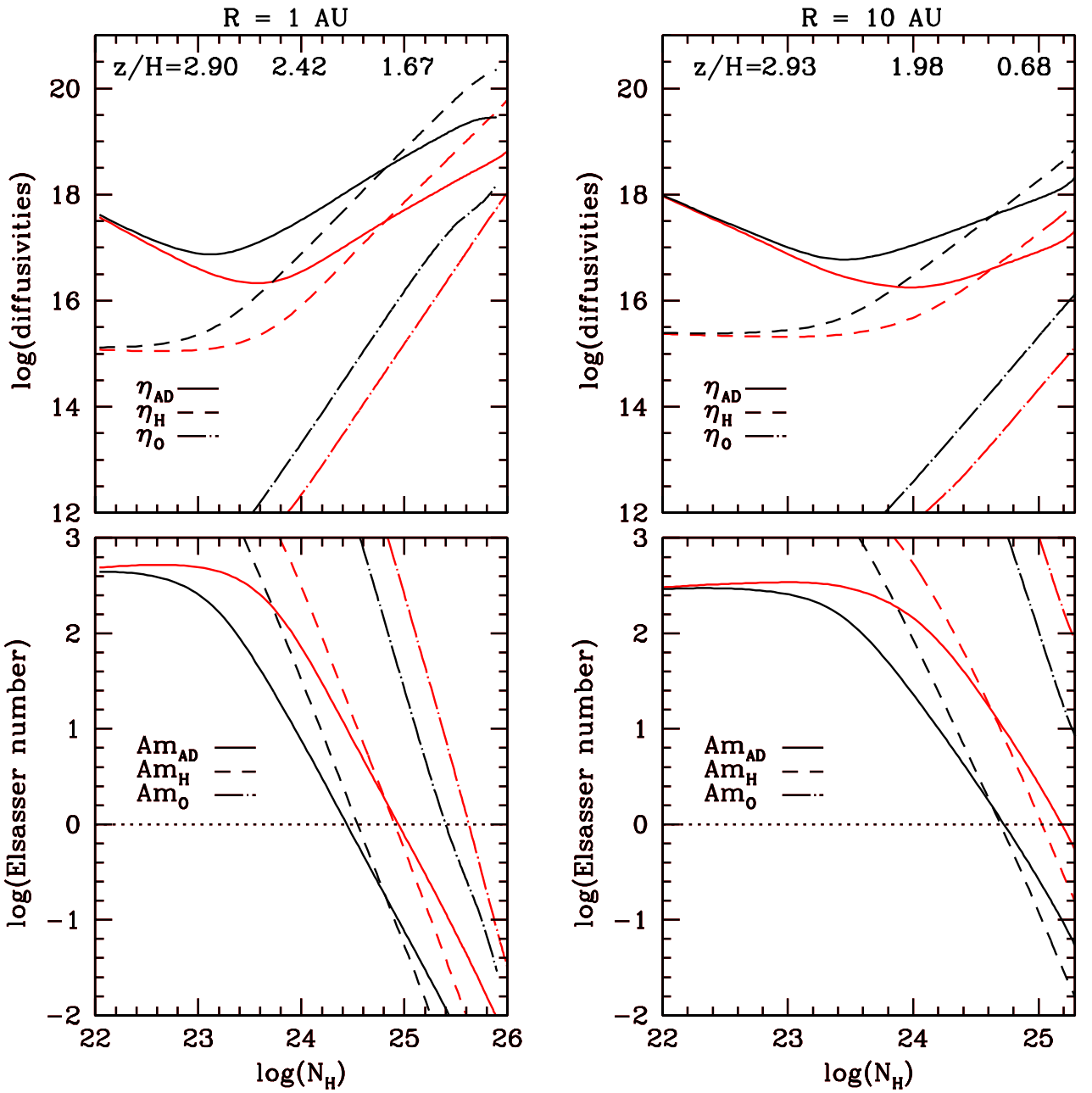

Figure 3. Diffusivities and Elsasser numbers calculated for a weakly magnetized T Tauri disk with a mass-to-flux ratio $\lambda = 12$, at disk radii $R = 1$ AU (*left panels*) and $R = 10$ AU (*right panels*), for grains with sizes $a = 10$ μm (*black curves*) and $a = 100$ μm (*red curves*). The solid lines correspond to the Ambipolar diffusion terms $\mathrm{Am_{AD}}$ and η_{AD}, the dashed lines correspond to the Hall terms $\mathrm{Am_H}$ and η_{H}, and the dot-dashed lines correspond to the Ohm terms $\mathrm{Am_O}$ and η_{O}. Note that the mid-plane column density at 10 AU is smaller than the mid-plane column density at 1 AU. The top axis in the top panels correspond to the number of scale heights is z/z_H at each column density (see text). For these models, $H(1\ \mathrm{AU}) = 2.25 \times 10^{-2}$ AU and $H(10\ \mathrm{AU}) = 2.78 \times 10^{-1}$ AU.

Figure 3 plots the three diffusivities and Elsasser numbers vs. vertical column density for two radii, 1 AU and 10 AU, and two grain sizes, $a = 10$ (black lines) and 100 μm (red lines). Focusing on the Elsasser numbers on the lower panels of Figure 3, they all decrease monotonically with N_{H}. At high altitudes, their numerical values satisfy the sequence: $\mathrm{Am_{AD}} < \mathrm{Am_H} < \mathrm{Am_O}$, but this can change deeper down. The usual interpretation of the two Elsasser numbers, $\mathrm{Am_O}$ and $\mathrm{Am_{AD}}$, comes from shearing-box simulations with large plasma β (weak fields). It is based on the idea that large $\mathrm{Am_O}$ guarantees that the ionized disk plasma is well coupled to the magnetic field, whereas large $\mathrm{Am_{AD}}$ guar-

antees that the ions are well coupled to the neutrals. Many authors found that the MRI is active if the Elsasser numbers are > 100, but others have advocated the condition > 1 (e.g., Bai & Stone 2011, Bai 2015). If we were to adopt the value of 1, then Figure 3 suggests that $\mathrm{Am_O}$ is probably large enough to provide good field-plasma coupling over much of the disk between 1 and 10 AU, but $\mathrm{Am_{AD}}$ is not large enough to provide adequate coupling of ions and neutrals over much of the disk. The steep slopes of the Elsasser numbers in this figure suggest that such deductions may depend on the choice of the critical number for the MRI. However, there will still be dead zones in the present case. Furthermore, the size of the dead zone is smaller for larger grains. Flock et al. (2012) carried out a global zero net-flux simulation that indicates that the MRI can be sustained with Elsasser numbers as low as 0.1. Even with this small value, however, dead zones still arise at 1 AU in the present model. In this context, it should be noted that the weakly-magnetized T Tauri disk model star considered here is fairly thick with a mid-plane thickness of $540\,\mathrm{g\,cm^{-2}}$; thinner disks may well have no dead zones. The upper axis of the diffusivity panels in the figure show the number of scale heights at a given column density. As in the case of isothermal disks, we chose the scale height H as the value of the height z that contains 68% of the surface density, measured from the mid-plane. For $R = 1$ AU, $H = 2.25 \times 10^{-2}$ AU, such that $z/H = 3.55, 2.90, 2.42$ and 1.67 for $\log N_H = 22, 23, 24$ and $25\,\mathrm{cm^{-2}}$. For $R = 10$ AU, $H = 2.78 \times 10^{-1}$ AU, such that $z/H = 4.00, 2.93, 1.98$ and 0.68 for $\log N_H = 22, 23, 24$ and $25\,\mathrm{cm^{-2}}$.

The present model considers a single ionization source, stellar X-rays, for the region below the FUV zone. As noted in Secs. 1 & 2, the X-ray ionization rate becomes uncertain beyond a certain depth, e.g., $\log N_{\mathrm{H}} = 25.25$ at 1 AU. There has been much speculation on the possibility of other ionization sources close to the mid-plane. In addition to stellar and galactic cosmic rays, locally-generated energetic particles may generate sufficient ionization to reduce the amount of MRI-dead material (e.g., Turner & Drake 2009; see also Gounelle 2015 for the role of radioactive nuclides and Ilgner & Nelson 2008 for the potential role of mixing). MRI turbulence itself may play a role here, as discussed recently by Inutsuka & Sano (2005) and Okuzumi & Inutsuka (2015).

The Hall length L_{H} as function of vertical column density is shown in Figure 4 for $R = 1$ and 10 AU and $a = 10$ and 100 μm. Eq. (32) for the Hall length indicates that it is inversely proportional to $\mathrm{Am_H}$. The small values of $\mathrm{Am_H}$ approaching the mid-plane in Figure 3 mean that L_{H} is much larger than the disk scale-height at the disk mid-plane. This is consistent with the generally accepted idea that the PPDs are significantly affected by the non-ideal MHD Hall term. The Hall length in these models is larger than the values obtained by Lesur et al. (2014) in their Figure 3, because of the different disk models, and also because of their higher ionization fraction due to the inclusion of cosmic ray ionization.

The discussion of Figure 3 emphasizes the occurrence and size of MRI dead zones. A corollary to the conclusion that thicker disks can have dead zones deep down, is that the MRI may still be active over a large volume of a T Tauri star disk. The turbulence associated with the MRI has long been considered to play a key role in angular momentum transport (e.g., Hawley & Stone 1998, Bai & Goodman 2009 and Mohanty et al. 2013), where the ionization is critical for the MRI. More recently, the transport of angular momentum has focused on the important role of disk winds (e.g., Bai et al. 2016, Bai 2016, Bai & Stone 2017). Although the thermal-chemical properties of the upper part of the disk (including the ionization) are important in this connection, the present theory of of deep-down ionization will not be relevant unless the base of the wind extends well below the FUV layer.

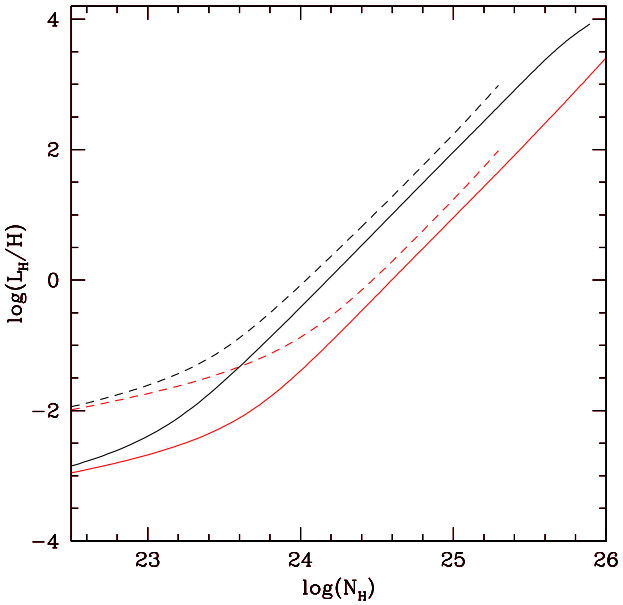

Figure 4. Ratio of the Hall length to the disk scale height H as function of vertical column density at $R = 1$ AU (*solid curves*) and 10 AU (*dashed curves*), for $a = 10$ μm (*black curves*) and 100 μm (*red curves*).

5 SUMMARY

By applying the methodology of Oppenheimer & Dalgarno (1974) (see also Ilgner & Nelson 2006a,b and Bai & Goodman 2009), we have obtained a simple description of the deep-down X-ray ionization of protoplanetary disks. The key step is to treat a small set of generic species, molecular ions like $\mathrm{HCO^+}$ and $\mathrm{H_3O^+}$ (represented by m^+), heavy atomic ions like $\mathrm{Na^+}$ and $\mathrm{Mg^+}$ (represented by M^+), and charged grains (g^-), as well as electrons (x_e). Below the FUV irradiated surface region, the ionization is described by a cubic equation in x_e. Over much of the inner disk, the vertical variation of the ionization follows simple closed-form expressions that are essentially power laws in vertical column density. We have illustrated the theory by calculating the Elsasser numbers for the standard non-ideal MHD effects for the weakly-magnetized T Tauri star disk model of Lizano et al. (2016). We foresee other applications of the theory to 2-d and 3-d MHD modeling of magnetic disks.

Another key aspect of the theory is the inclusion of the reactions whereby atomic ions transfer their charge to grains. This process has been ignored in some MRI simulations, with the result that $x_e = (\zeta_X/\beta n_{\mathrm{H}})^{1/2}$, where β is

the dissociative recombination rate coefficient for molecular ions. This expression produces too small values of x_e near the mid-plane of moderately thick disks (see instead eq. 25).

The present application would seem to suggest that fairly thick disks, approaching the thickness of the MMSN have dead zones even with X-ray ionization. This raises an important limitation of the theory in that the level of ionization deep down, e.g., beyond log $N_{\rm H} = 25$, is uncertain. This is mainly due to the limitations in the Monte Carlo propagation of the scattered X-rays and our incomplete understanding of the blocking of galactic cosmic rays by the angular-dependent stellar wind. And beyond these major uncertainties, there may be additional internal sources of ionization, such as the MRI itself.

ACKNOWLEDGMENTS

S. L . acknowledges support from PAPIIT-UNAM IN105815 and CONACytT 238631.

REFERENCES

Ádámkovics, M., Glassgold, A.E., & Najita, J.R. 2016, ApJ, 817, 82
Ádámkovics, M., Najita, J.R. & Glassgold, A.E., 2014, ApJ, 736, 144
Anderson, D.E., Bergin, E.A., Maret, S. & Wakelam, V., 2013, ApJ, 779, 141
Anicich, V. G. 1993, Journal of Physical and Chemical Reference Data, 22, 1469
Bai, X.-N., & Stone, J. M. 2017, ApJ, 836, 46
Bai, X.-N. 2016, ApJ, 821, 80
Bai, X.-N., Ye, J., Goodman, J., & Yuan, F. 2016, ApJ, 818, 152
Bai, X.-N. 2015, ApJ, 798, 84
Bai, X.-N., & Goodman, J. 2009, ApJ, 736, 144
Bai, X.-N., & Stone, J. M. 2011, ApJ, 701, 737
Balbus, S. A., & Hawley, J. F. 1991, ApJ, J. 376, 214.
Cleeves, L. I., Adams, F. C., & Bergin, E. A. 2013, ApJ, 772, 5
Draine, B. T., & Sutin, B. 1987, ApJ, 320, 803 (DS87)
Ercolano, B. & Glassgold, A.E. 2013, MNRAS, 436, 3446
Flock, M., Henning, T., & Klahr, H. 2012, ApJ, 761, 95
Gammie, C. F. 1996, ApJ, 457, 355
Glassgold, A.E., Najita, J. & Igea, J. 1997, ApJ, 480, 344
Gounelle, M. 2015, A&A, 582, A26
Hayashi, C. 1981, Prog. Theor. Phys., 70, 35
Hawley, J. F., & Stone, J. M. 1998, ApJ, 501, 758
Igea, J. & Glassgold, A.E., 1999, ApJ, 518, 844
Ilgner, M., & Nelson, R. P. 2006a, A&A, 445, 205
Ilgner, M., & Nelson, R. P. 2006b, A&A, 445, 223
Ilgner, M., & Nelson, R. P. 2008, A&A, 483, 815
Inutsuka, S.-I. & Sano, T. 2005, ApJ, 628, L155
Joseph, C.L., Snow, T.P., Seab, C.G., & Crutcher, R.M. 1986, ApJ, 309, 771
Lesur, G., Kunz, M.W., & Fromang, S. 2014, A&A, 817, 35
Lizano, S., Tapia, C., Boehler, Y., & D'Alessio, P. 2016, ApJ, 817, 35
Mathis, J. S., Rumpl, W., & Nordsieck, K. H. 1977, ApJ, 217, 425
Mohanty, S., Ercolano, B., & Turner, N. J. 2013, ApJ, 764, 65
Nakano, T., Nishi, R., & Umebayashi, T. 2002, ApJ, 573, 199
Najita, J. R. & Ádámkovics, M. 2017, ApJ, submitted
Okuzumi, S., & Inutsuka, S.-I. 2015, ApJ, 800, 47
Oppenheimer, B. & Dalgarno, A. 1974, ApJ, 192, 29
Pinto, C., Galli, D., & Bacciotti, F. 2008, A&A, 484, 1
Pinto, C., & Galli, D. 2008a, A&A, 484, 17
Pinto, C., & Galli, D. 2008b, A&A, 492, 1
Savage, B.D. & Sembach, K.R. 1996, ARAA, 34, 279
Shu, F. H., Galli, D., Lizano, S., Glassgold, A. E., & Diamond, P. H. 2007, ApJ, 665, 535
Spitzer, L. 1978, Physical processes in the interstellar medium, New York Wiley-Interscience, p. 333
Spitzer, L. 1941, ApJ, 93, 369
Turner, N. J., & Drake, J. F. 2009, ApJ, 703, 2152